Experiment on collisionless plasma interaction with applications to supernova remnant physics

C. Courtois, R. A. D. Grundy, A. D. Ash, D. M. Chambers,[a] and N. C. Woolsey
Department of Physics, University of York, York YO10 5DD, United Kingdom

R. O. Dendy and K. G. McClements
UKAEA Culham Division, Culham Science Centre, Abingdon OX14 3DB, United Kingdom

(Received 25 February 2004; accepted 22 March 2004; published online 27 May 2004)

Results from an experimental study of the collisionless interaction of two laser-produced plasmas in a magnetic field with applications to supernova remnant shock physics are presented. The dynamics of the two plasmas and their interaction are studied with and without magnetic field through spatially and temporally resolved measurements of the electron density. Experimental results show that counter-propagating collisionless plasmas interpenetrate when no magnetic field is present. In contrast, results obtained with the addition of a 7.5 T magnetic field perpendicular to plasma flow show density features in the interaction area that only occur when the field is present. The reason for this remains uncertain. It is suggested that this results from an increase in the effective collisionality as the magnetic field reduces the ion and electron gyroradius below the size of the experiment. [DOI: 10.1063/1.1752930]

I. INTRODUCTION

High-power laser-plasma experiments have been used to test models of space and astrophysical interest for some time. Experiments have studied both hydrodynamic properties[1–3] and radiative properties[4] of plasmas as illustrated in the reviews by Ripin *et al.*,[1] Remington *et al.*,[2] Takabe *et al.*,[3] and Rose.[4] Laser-plasma results have been applied previously to the study of such diverse phenomena as active galactic nuclei[5] and the Earth's bow shock.[6] The relevance of these laboratory experiments to astrophysical phenomena relies on a detailed scaling analysis, based on a scale invariant magnetohydrodynamics (MHD) model.[7] If certain dimensionless parameters are matched between an experiment and the astrophysical object of interest, the existence of such a model ensures that the same physics operating in the astrophysical object is reproduced in the laboratory. This offers the opportunity to test against experiment astrophysical plasma modeling used to interpret observation; furthermore, an experiment can be used to test the model robustness through the controlled modification of the input conditions, and the ability to make repeated detailed measurements.

A particular set of astrophysical problems is associated with the plasma physics of collisionless shock formation, particle acceleration, and cosmic ray transport in supernova remnants (SNR).[8] These collisionless shocks occur in magnetized plasmas when ejected stellar matter from a supernova interacts at high speed, initially with the circumstellar medium and then later the interstellar medium. Energy dissipation in these collisionless shocks, and the acceleration mechanisms believed to be present, result in cosmic rays with energies up to 10^{15} eV.[8]

In a previous article,[9] we identified a set of key parameters for a typical reverse shock in a young SNR, and by applying ideal MHD demonstrated that these parameters may be matched by a laser-plasma experiment. The objective of the present experiment is to scale a collisionless SNR shock at a certain time after the supernova explosion and then to recreate plasma conditions close to this shock in the laboratory. We have chosen to investigate a SNR at one instant, 100 years following the supernova event. This is believed to be an important period during the evolution of a SNR shock and for the seeding of cosmic rays.[10] Creating laboratory conditions similar to those at a supernova remnant shock, and diagnosing the physical processes occurring, is clearly of interest.

The principle of the experiment is based on the interaction of two counter-streaming, or opposing, supersonic expanding plasmas produced from laser-exploded foils. The exploding plasmas are immersed in an external magnetic field. The scaled conditions are achieved approximately 500 ps after laser irradiation. In this case we are interested in (quasi) perpendicular shocks where the magnetic field is transverse to the plasma flow. By irradiating thin plastic foils with intense laser beams, a high velocity expansion is achieved. To ensure a collision-free experiment it is necessary to work with a low atomic number target material, and high plasma expansion speed. This combination is used to ensure that the counter-streaming particle collisional mean free paths (mfp) exceed the size of the experiment, which is about 1 mm. The role of the external magnetic field is to introduce new physics, associated with length scales shorter than the mfp—namely the ion and electron gyroradius. If these new scale lengths are sufficiently small the collision-free, magnetized plasma, may behave like a fluid with an effective collisionality. Plasma heating will result from interactions between these counter-streaming plasmas, increasing the ion gyroradius.

The remainder of this paper is organized as follows. Scaling of an experiment to a SNR is described in Sec. II, the

[a]Present address: AWE, Aldermaston, Reading, RG7 4PR, United Kingdom.

TABLE I. Comparison of the scaling parameters for the reverse shock in a young SNR (Ref. 10) and the experimentally derived values measured at 500 ps.

Parameters	SNR 100 y	Expt. 500 ps
Collisionality, ζ	2×10^{6}	3×10^{2}
Plasma beta	$\beta=5\times10^{2}$	$\beta^{*}=4\times10^{2}$
Euler number, Eu	18	21
Mach number, M	16	12
Alfvén Mach, M_A	3×10^{2}	20
Ion localization, r_{Li}/L	10^{-9}	10^{-1}
Reynolds number, R_e	10^{13}	10^{7}
Peclet number, P_e	10^{11}	10^{10}

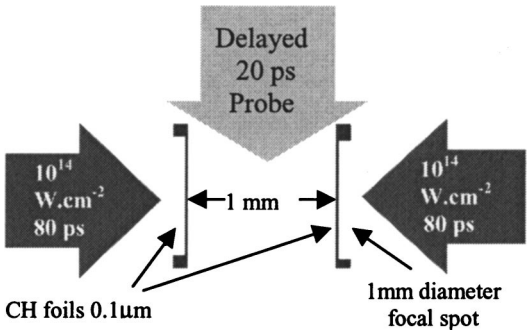

FIG. 1. Opposing foil target geometry and laser probe alignment. The probe is delayed relative to the peak of the drive lasers by 250 to 750 ps. The magnetic field orientation is down the page, perpendicular to the plasma flow.

experimental setup is described in Sec. III, and experimental results are presented in Sec. IV. In Sec. V, these results and the matching of the scaling conditions are assessed, and conclusions are given in Sec. VI. All expressions are written in SI.

II. SCALING

Typically, laser-plasma experiments and astrophysical plasmas differ by many orders of magnitudes in temporal and spatial scales. In designing an experimental simulation, these differences are considered by identifying a similarity principle that allows a direct scaling and thus a direct comparison. For example, through the use of invariant properties of various plasma models, different experiments have been directly compared, as illustrated by Connor and Taylor.[11] More recently this type of analysis has been extended by Ryutov *et al.*[7] to enable the comparison of laser-plasma experiments with astrophysical systems such as supernovae and SNRs. Scaling of the dynamics of a fluid is appropriate if the ideal fluid (e.g., Euler) equations can be applied to the hydrodynamics of both the astrophysical object and the experiment. Similarly, scaling of collisionless plasma phenomena is possible if the magnetized ideal fluid (MHD) equations apply.

A set of SNR parameters, typical for the reverse shock, a shock propagating back into the stellar ejecta, in young SNR,[10] used for scaling is shown in Table I. These are the parameters that must be matched by an experiment, in addition to a set of assumptions that are discussed below. The experimental parameters are shown for the laser plasma experiment at 500 ps; how these values are inferred will be discussed in Sec. V following presentation of the results. The scaling parameters are identified under the assumption of ideal MHD. This imposes four essential considerations. First, the plasma must be collisionless. This is characterized by a collisionality parameter, ζ, the ratio of the ion collisional mfp to a typical scale length, which must be much larger than 1.

Second, the application of Euler equations assumes that plasma behaves like a fluid and that dissipative effects such as thermal conductivity and viscosity are negligible. To apply the Euler equations a plasma must exhibit a very large Peclet number, $P_e=vL/\chi$, and a very large Reynolds number, $R_e=vL/\chi_h$. Here v and L are a characteristic fluid speed and system size, respectively, and χ the thermal diffusivity and χ_h the viscosity. Despite the absence of collision, for example, in the SNR where $\zeta>10^{6}$ (see Table I), a fluid model can be applied if a magnetic field results in particle gyroradii that are smaller than the system scale length,[12] this gives rise to an effective collisionality.

Third, the Euler equations are invariant under "Euler transformation"[7,11] which conserves the Euler number, $\mathrm{Eu}=v(\rho/p)^{1/2}$, where v is any suitable characteristic velocity of the system, p is the plasma pressure, and ρ is the mass density. It is interesting to note that dissipative structures such as shocks are allowed in this scale transformation.[7] In addition, to establish invariance of the ideal magnetized fluid equations, the ratio of the thermodynamic pressure to magnetic pressure must be preserved, i.e., the plasma beta $\beta=2\mu_0 p/B^2$, where μ_0 is permeability of free space and B the amplitude of the magnetic field, is conserved. A SNR is typified by a large β, indicating that the magnetic field does not dominate the global fluid motion of the plasma, however this magnetic field introduces the ion gyroradius, r_{Li} as an additional fundamental scale length. Thus the hydrodynamics of the SNR and the role of the magnetic field on its evolution can be simulated in the laboratory by matching the experimental Eu and β parameters. This transformation was identified by Connor and Taylor and labeled "E_2."[11]

Fourth, to ensure that a strong shock is formed, the Alfvénic Mach number $M_A=U_f(\mu_0\rho)^{1/2}/B$ and the sonic Mach number $M\approx U_f(\rho/p)^{1/2}$ must be greater than unity (here U_f is the bulk fluid speed).

III. EXPERIMENT

An outline of the experiment is reproduced in Fig. 1. Here two face parallel, 100 nm thick C_8H_8 foils are mounted across a 1.2 mm hole on either 50 μm thick copper or 250 μm thick Mylar washers separated by 1 mm, the characteristic size of the system, L. The foil targets are grown by thermal evaporation, and mounted on washers by surface tension. The targets are heated to remove any foil structure; foil thicknesses are known to 10% accuracy. Mylar washers were used for some of the shots without magnetic field and for all the shots with magnetic field. This was to prevent possible field disturbance due to eddy currents induced in the target holder. These foils are irradiated simultaneously with 1

or 2 intense laser beams per foil at peak intensity of 0.6 or $1.2\times10^{14}\,\mathrm{W/cm^2}(\pm10\%)$, with an 80 ps duration laser pulse and 1.053 μm wavelength. Plasmas are created and accelerated by irradiating the nonopposing surfaces of the two foils. Phase zone plates are used to spatially smooth laser focal spot profiles and increase the spot diameter on the target foil to 1 mm. The spot diameter is twice the expansion distance to the interaction point; this allows the plasma to be approximated with a one-dimensional planar expansion. The one-dimensional planar expansion is used in the data analysis, where the plasma is assumed to be cylindrically symmetric.

For experiments requiring the use of a magnetic field, the foils are placed at the center of a pulsed electromagnet producing a uniform 7.5 T magnetic field of 1 ms duration. The electromagnet design restricted laser access to one laser beam per target foil. The magnetic field orientation is perpendicular to the plasma flow and parallel to the initial target foil surface. The magnetic field is chosen to ensure that the plasma β remains larger than 1, as such it is not expected to affect the expansion of the exploding plasma. In addition, this magnetic field is sufficiently large to ensure that the electron and ion gyroradii are the shortest scale lengths of interest, and small compared to the spatial extent of the experiment. If collisionless heating does occur, the ion gyroradius, which is proportional to the square root of the ion temperature, T_i, will increase and exceed the experimental size at $T_i\sim10\,\mathrm{keV}$.

The plasma expansion is studied with a 25 ps duration, frequency doubled laser probe beam with wavelength at 0.53 μm. This beam is spatially smoothed to ensure a high quality near field, and then passes between the foils, parallel to the foil surfaces and perpendicular to the one-dimensional plasma flow. This probe can be delayed relative to the main laser beams forming the plasmas, and is used to record a series of snapshots of the time evolution of the expanding plasmas from separate experiments. In addition, the polarization of the probe beam is fixed at 45° relative to the foil surfaces with a high extinction ratio ($1{:}10^5$) Glan–Taylor prism polarizer; this is placed immediately before the experimental chamber. The probed plasma is imaged by an f6 achromat lens and analyzed using a modified Normarski interferometer based on a polarization splitting Wollaston prism. The minimum and maximum electron densities probed are limited by the smallest measurable fringe shift and the effective aperture of the f6 optical system, respectively, and are $5\times10^{17}\,\mathrm{cm^{-3}}$ and $5\times10^{19}\,\mathrm{cm^{-3}}$ along a 1 mm chord through the plasma, respectively.

The ion temperature, T_i, is estimated from spectroscopic measurements of the thermally broadened helium-like carbon (C^{4+}) lines $1s2s\,^3S_1-1s2p\,^3P_{2,1,0}$ triplet transition centered at 227 nm. Additional data are provided by ion time of flight measurements using a series of Faraday cups placed around the target. Ion temperature estimation assumes a Maxwell–Boltzmann distribution for the ion population. The pressure in the experimental chamber is maintained at $10^{-4}\,\mathrm{mbar}$.

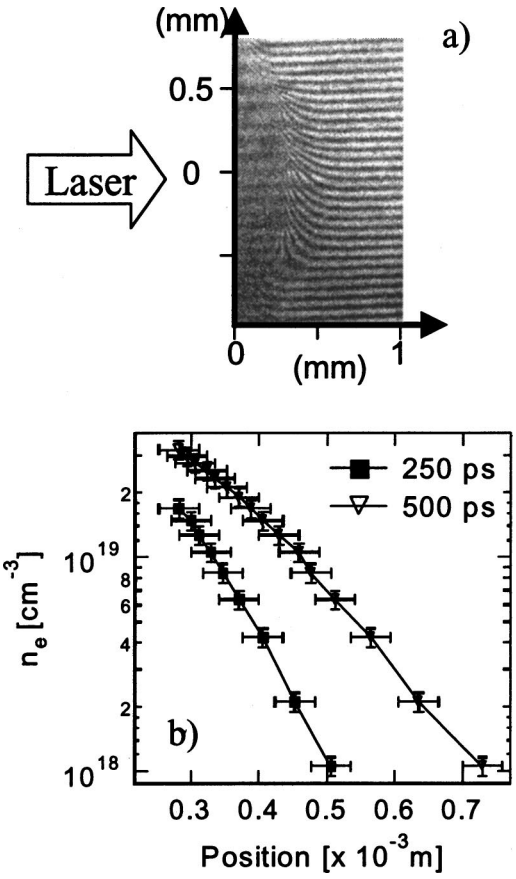

FIG. 2. Interferograms of one exploding foil at 250 ps delay (a), 79 J energy. (b) shows the horizontal profiles of electron density at the center of the foil at 250 ps, solid square points, and 500 ps, open triangle points, as a function of distance from the initial foil target position.

IV. EXPERIMENTAL RESULTS

In this section interferometric data are described. These data are recorded as 25 ps duration snapshots, taken between 250 ps and 1 ns after the peak of the laser pulse used to drive the explosion of the plastic foil targets. First, in Sec. IV A we present data on single foil plasmas to demonstrate supersonic expansion of the plasmas and demonstrate that the magnetic field does not affect the plasma hydrodynamics. In Sec. IV B the counter-streaming data are presented, these data indicate that the magnetic field does affect the plasma behavior. The quoted laser energies on target are known to $\pm10\%$.

A. Plasma expansion from one exploding foil

An example of interferometric data of one exploding foil target is shown in Fig. 2(a). This measurement was recorded with a probe delay of 250 ps and without a magnetic field. This interferometer image is recorded after the laser pulse (FWHM of 80 ps), which approaches from the left-hand side of the Fig. 2(a). The center of the laser spot in Fig. 2(a) corresponds to the position 0 on the vertical axis. The horizontal axis shows the region from the initial foil position, at 0, and the region behind the foil. Dark areas without fringes appear in the left portion of the interferograms, these areas are due to refraction of the laser probe on the high gradients in the denser part of the expanding plasma. These areas are

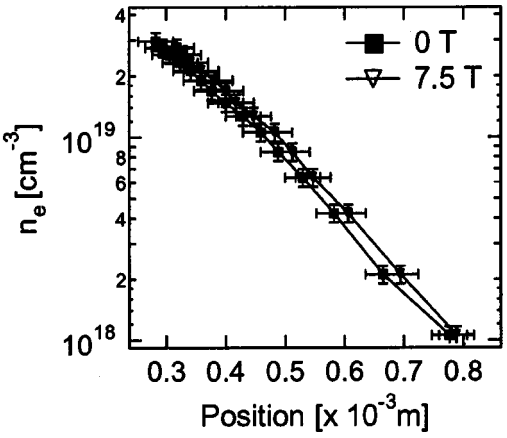

FIG. 3. Horizontal profiles of electron density at the center of the foil at 750 ps delay, without, square points, 42 J energy and with, triangle points, 39 J energy, a 7.5 T magnetic field, as a function of distance from the initial foil target position.

below critical density. The regions where interference fringes are clearly seen are areas where the refractive index gradient is sufficiently low that the refracted laser probe is still collected by the optical system. Visual inspection of these fringes indicates that the plasma expansion is uniform. Uniform plasmas and uniform expansion are important to ensure that the physical processes of interest are not masked by structure in the plasma. The necessary uniformity is achieved by smoothing the laser intensity distribution with phase zone plates (PZP) and by controlling the film uniformity and flatness of the foil targets.

In Fig. 2(b) the inferred central horizontal electron density, n_e, of the expanding plasma is shown for two different probe delays. These results assume that the plasma is a uniform 1 mm thick slab. Data from two interferograms recorded at 250 ps and 500 ps are compared and indicated, respectively, by solid squares and open triangles. Position 0 corresponds to the initial foil target position; the electron density is shown between 0.2 mm and 0.8 mm from foil position (data for the first 0.2 mm are not available due to refraction). In addition to the density measurements, we have inferred the plasma expansion speed, V_{exp}, of the leading edge directly from the interferograms. The leading edge is fixed as the position of first quarter of fringe shift; this corresponds to an electron density of $10^{18}\,\mathrm{cm}^{-3}$. We find that at 500 ps $V_{\mathrm{exp}}=1.5\times10^{8}$ cm/s($\pm10\%$) with two incident laser beams ($\sim$80 J on target) and $V_{\mathrm{exp}}=1.1\times10^{8}$ cm/s($\pm10\%$) with one beam ($\sim$40 J). The use of thin, $\sim$100 nm thick, plastic foil targets results in the production of a fast expanding plasma with low density and low atomic number. This is important for achieving a collision free interaction in a counter-streaming experiment.

In Fig. 3 density profiles of one exploding foil without and with a 7.5 T magnetic field are compared. These measurements are made at a relatively long probe delay of 750 ps, so as to determine what effect the magnetic field may have on the exploding plasma hydrodynamics. Both experiments used similar plastic foil targets and were exploded with one laser beam containing 42 J and 39 J, respectively. Magnetic field free data are represented by the solid squares

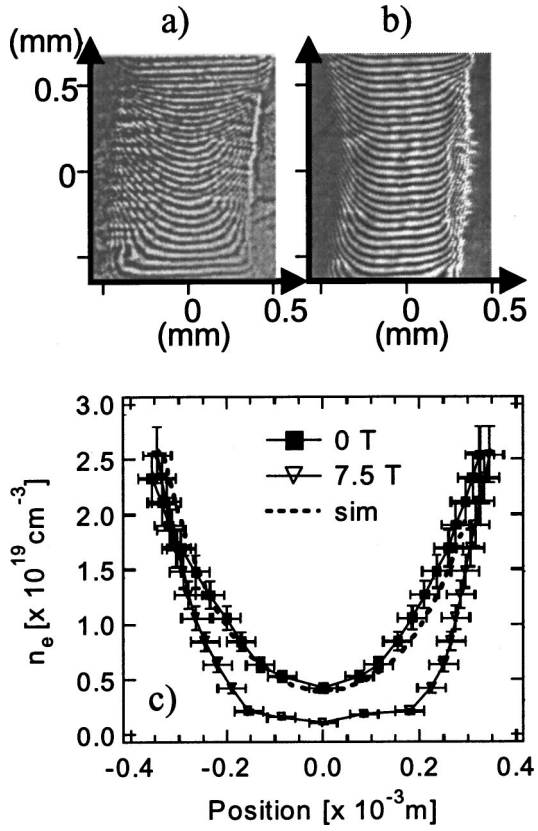

FIG. 4. Interferograms of two exploding foils at 500 ps delay (a) without magnetic field (41 J on left foil, 44 J on right foil); (b) with a 7.5 T magnetic field (41 J on left foil, 50 J on right foil). (c) Horizontal profiles of the electron densities at the center of the foil without (square) and with (triangle) B field. The dashed line is constructed from two single foil measurements as discussed in Sec. V.

and 7.5 T data by open triangles. The inferred electron densities extracted from the central region of the foils are identical. These results indicate that the magnetic field does not affect the hydrodynamic expansion of single foil plasmas up to 750 ps time delay, nor for distances of propagation comparable to foil target separation when used in the opposing plasma geometry (i.e., $\sim$1 mm).

B. Counter-streaming plasma interaction

In the counter-streaming experiments, two foil targets separated by 1 mm are simultaneously exploded. Examples of interferograms are shown in Fig. 4, the probe delay is 500 ps in both cases. Figure 4(a) shows the result for a magnetic field free experiment with 41 J on the left foil and 44 J on the right foil. Figure 4(b) shows results from a comparable experiment but with a 7.5 T magnetic field. Laser beams come from the left-hand and right-hand sides of each interferogram, with the initial foil positions corresponding to the positions -0.5 and 0.5 mm on the horizontal axis. The counter-streaming plasmas interact in the central part of each image. A comparison of these images indicates that the presence of a magnetic field does make a difference. For example, there are curved fringes in Fig. 4(a) and flattened fringes in the central region of Fig. 4(b). The inferred electron density profiles are taken from the central horizontal region of both

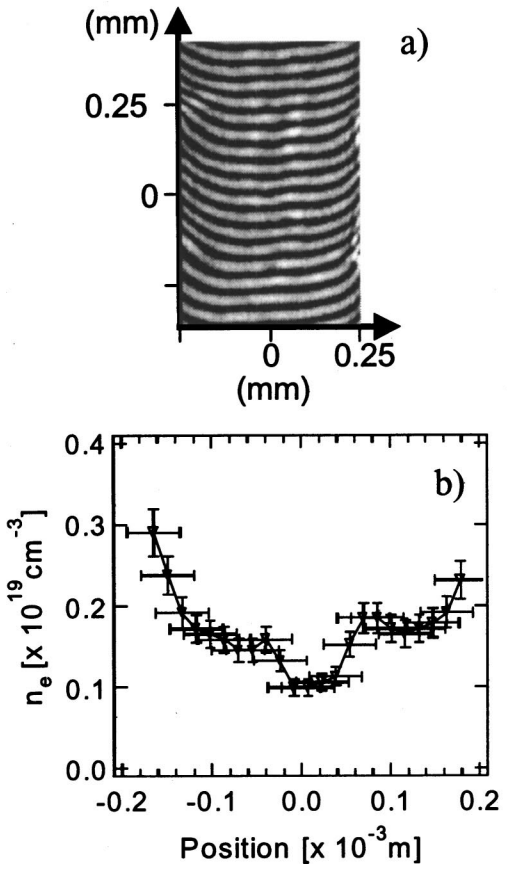

FIG. 5. An enlargement of the center of Fig. 4(b). (a) shows the interaction area and (b) shows the inferred n_e about the mid-point of the experiment.

images and assume the plasmas are 1 mm thick, and are shown in Fig. 4(c). The magnetic field free data are indicated by the solid square markers and have a parabolic profile. The position zero corresponds to the experimentally determined minimum interference fringe shift, with an inferred $n_e = 4.2 \times 10^{18}\,\mathrm{cm}^{-3}(\pm 10\%)$. These inferred densities are consistent with the density profiles measured from single foil experiments.

In contrast, the inferred electron density profile obtained with a 7.5 T magnetic field, indicated by open triangles in Fig. 4(b), is characterized by a steepened gradient close to the foil targets initial position and by a low-density $[n_e = 1 \times 10^{18}\,\mathrm{cm}^{-3}(\pm 10\%)]$, low-gradient 350 μm wide area centered on the mid-point between the foil targets. This is the region where the two plasmas interact. This result is in contrast to those presented in Fig. 3 where the single plasma profiles are independent of a magnetic field up to 7.5 T. It appears that the 7.5 T magnetic field does affect the two counter-streaming plasmas, this will be discussed in greater detail in Sec. V.

The central region of Fig. 4(b) is enlarged in Fig. 5(a) and more detailed measurements of the inferred electron density are shown in Fig. 5(b). These figures highlight additional density structure. The two bright features on the interferogram, with widths around 150 μm, correspond to a small increase in electron density at either side of the density minimum. Features similar to these are observed only when the magnetic field is present.

Spectroscopy measurements of the C^{4+} line without magnetic field present indicate that the ion temperature is around 180 ± 20 eV for both single plasmas and counter-streaming plasmas. This indicates that no significant heating of the ions occurs when counter-streaming plasmas interact. It has not been possible to estimate the ion temperature in the presence of magnetic field; this is due to additional noise introduced on firing the electromagnet.

V. DISCUSSION

In this section we determine the experimental scaling parameters and compare these to those defined for the reverse shock of a young SNR and shown in Table I. The role of the magnetic field in the single plasma and opposing plasma experiment is discussed, and finally we propose how the magnetic field affects the experiment. The experimental results are also discussed in relation to numerical simulations produced using the one-dimensional Lagrangian hydrodynamic laser-plasma model Med103.[13]

The sensitivity of the experimental scaling parameters to experimental uncertainty is estimated by numerical simulation. Med103 is used to simulate the hydrodynamic expansion of a plasma created from a 100 nm thick plastic (C_8H_8) foil irradiated by a laser beam with a Gaussian pulse 80 ps FWHM duration, 1.053 μm wavelength, and $5 \times 10^{13}\,\mathrm{W/cm}^2$ peak laser intensity. The simulation uses flux limited heat transport for both the electrons and ions. We use the average atomic number and mass number for the plastic foil target of 3.5 and 6.5. In the following figures, solid lines indicate the numerical results and are compared with two thin dotted lines. These dotted lines indicate the influence of varying the laser energy and foil thickness by $\pm 10\%$ to account for experimental uncertainty. The laser energy is the most sensitive parameter. The solid dot represents plasma parameters estimated from experimental results taken at 500 ps and reported in Table I. Position 0 corresponds to the initial foil position, and time 0 to the peak of the laser pulse.

The right-hand column of Table I, is a set of experimental parameters, which are based on measurement taken 500 ps after foil target explosion. Table I shows that counter-streaming plasma interaction is collision free as indicated by the collisionality parameter $\zeta \gg 1$. This result is determined from the measured plasma flow speed and plasma density, and assumes the plasma is fully ionized. Data clearly indicate that interpenetration of the two plasma streams occurs, and that collisions are not important at the time of measurement between 250 ps and 750 ps. The near-parabolic shaped counter-streaming electron density profile with no magnetic field present in Fig. 4 supports this conclusion. This is reinforced by comparison with the artificial result constructed from the addition of two sets of single foil data, which mimics an interpenetrating flow. Furthermore, for our experimental conditions, collisionless coupling between the counter-streaming plasmas due to electrostatic instability[14] is not expected to occur.

The experimental ζ result is compared to simulation in Fig. 6. Here the simulated ζ is derived from the ion–ion

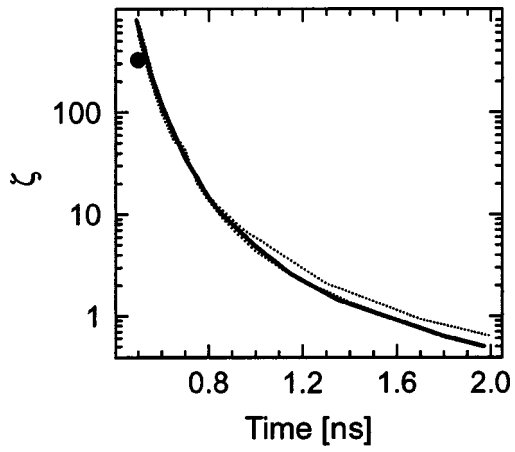

FIG. 6. The experimental (solid dot) collisionality parameter, ζ, at 500 ps and 0.5 mm from foil surface compared with simulated (thick solid line) versus time. Thin dotted lines represent a $\pm 10\%$ variation in simulated laser energy and foil target thickness; this is discussed in Sec. V.

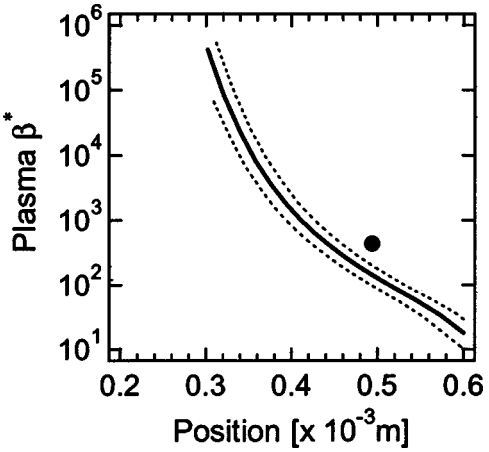

FIG. 7. The experimental (solid dot) plasma beta, β^*, at 0.5 mm and 500 ps, compared to the simulated β^* (thick solid line) versus distance from the foil target surface. Thin dotted lines are discussed in Sec. V.

mean free path (λ_{ii}) for two counter-streaming carbon plasmas estimated from hydrodynamics simulation[9] of a single carbon foil irradiated at $5\times10^{13}\,\mathrm{W/cm^2}$ and using an expression from Ref. 15, and a system size of 1 mm. For an average ionization of $Z=6$ (i.e., C^{6+}) and up to 1 ns, λ_{ii} is larger than 1 mm, this implies that any interaction between counter-streaming ions is collisionless. Since λ_{ii} scales as $1/Z^4$, the λ_{ii} for lower ionization stages and for H^+ will be higher and remain collision free. Figure 6 shows that both numerical and experimental results indicate collision-free plasma interaction at 500 ps.

The second parameter in Table I is the plasma β for the SNR, and a nonstandard definition of β for the experiment, which is denoted as β^*. The experimental β^* is determined from the flow speed, i.e., we consider the directed kinetic energy rather than the thermal kinetic energy, and the inferred electron density to estimate a ram pressure, and by adjusting the magnetic field strength to give the required match. A 7.5 T magnetic field ensured that an experimental $\beta^*=400$ was achieved at 500 ps. Figure 3 indicates that the evolution of the electron density for a laser-driven exploding single foil target is independent of whether a magnetic field up to 7.5 T is present or not, for at least 750 ps following laser explosion of the foil. This implies $\beta^*>1$. In Fig. 7 the experimental β^* is compared to a numerical β^* plotted as a function of position in the plasma, at one instant of 500 ps. To derive the numerical result it is necessary to estimate the penetration of an external magnetic field in to the plasma. Magnetic field penetration is an area of great uncertainty and controversy, and is discussed qualitatively. The results presented in Figs. 4 and 5 suggest magnetic penetration.

A magnetic field can penetrate a highly ionized plasma if the skin current drift velocity, induced by an external magnetic field, exceeds the local sound speed. In this situation ion–acoustic turbulence results, and electron scattering occurs to induce an anomalous resistivity. This mechanism results in an enhanced magnetic field penetration.[16] We assume that the current determined by microturbulence is equal to a limiting value $j=\alpha n_e e C_s$, where C_s is the sound speed, and the parameter α is of the order of unity and smaller than $(m_i/Zm_e)^{1/2}$. Here e is the electronic charge, m_i and m_e are the ion and electron masses, respectively, and Z the average ion charge. For conditions relevant here, we estimate the local magnetic field by integrating Ampère's law in slab geometry, assuming that magnetic field diffusion into the plasma occurs at a rate sufficient to ensure that the current remains at the limiting value.[17] These results are shown in Fig. 8 where the simulated electron density for a laser exploded foil target at 500 ps as a function of position is indicated by the solid line, and the amplitude of a penetrated magnetic field due to an applied 7.5 T magnetic field, B, is indicated by the thick dashed line represents after penetrating the plasma. This figure illustrates how a penetrated magnetic field is likely to attenuate in the plasma as the electron density increases. The model assumes relatively fast field diffusion when compared to hydrodynamic time. Magnetic field penetration occurs to within $0.3\times10^{-3}\,\mathrm{m}$ of the foil target surface at 500 ps, as shown in Fig. 8. This limit is determined by the diffusion time, estimated as 50 ps.[18] These results are used to derive the numerical β^* (derived from the plasma flow pressure) in Fig. 7, and illustrate how β^* is

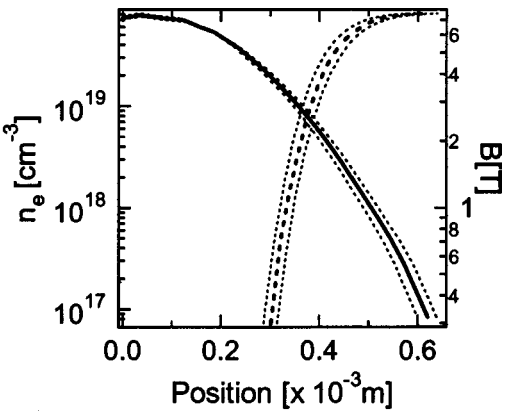

FIG. 8. Simulated electron density, n_e (thick solid line) and magnetic field amplitude (thick dashed line) at 500 ps versus distance from the foil target surface. Thin dotted lines are discussed in Sec. V.

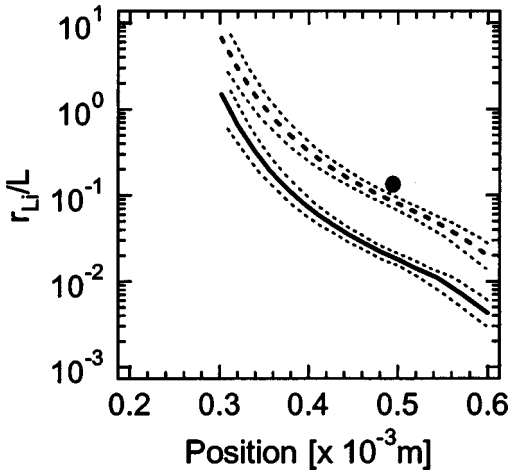

FIG. 9. The experimental ion localization parameter, r_{Li}/L (solid dot) at 0.5 mm and 500 ps, compared with simulated r_{Li}/L (thick solid line) as function of distance from the foil target surface. Thin dotted lines are discussed in the text.

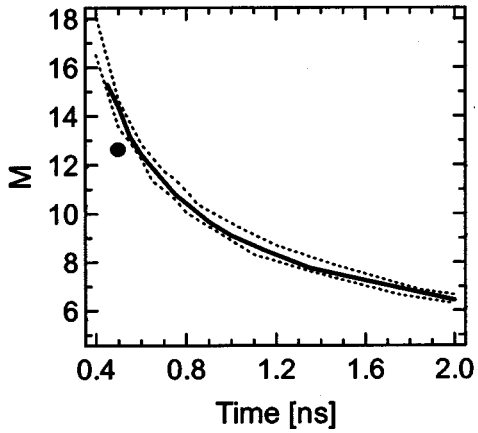

FIG. 10. The experimental Mach number, M (solid dot) at 0.5 mm and 500 ps compared to simulated M (thick solid line) at 0.5 mm and from foil target surface versus time. Thin dotted lines are discussed in the text.

expected to vary with position in the plasma. At 500 ps, β^* still exceeds unity 0.7 mm from the foil surface, indicating why the expansion of the plasma is not affected by this magnetic field. This is supported by data shown in Fig. 3.

The ion localization, r_{Li}/L, is the ratio of the shortest scale length of interest, in this case the ion gyroradius, to the system size. A magnetic field amplitude of 7.5 T is large enough to localize the ions $r_{\mathrm{Li}}/L<1$, if the ion temperature is sufficiently low (i.e., $T_i<10$ keV). Using the ion temperature measured from spectral line shapes and Faraday cup results, which are 180 ± 20 eV and ~100 eV, respectively, results in $r_{\mathrm{Li}}/L=0.1$. This experimental value, indicated by the dot in Fig. 9, is compared to simulation. Simulation predicts a low T_i of ~10 eV and T_e as 100 to 200 eV. The solid line indicates the simulated r_{Li}/L, and the thick dashed line in Fig. 9 indicates a second simulation with ion temperature artificially multiplied by 20, to be consistent with the experimentally measured temperature. Note that the simulated electron temperature is sufficient to ionize carbon to at least C^{4+}, and that C^{4+} is observed in the experiment.

The third parameter is the Euler number Eu. The experimental value estimated for Eu is 21, derived from measurements of plasma density, temperature, and expansion speed at 500 ps following the foil targets explosion. This is similar to the Eu derived for the SNR, indicating the experimental hydrodynamics approach the young SNR hydrodynamics at 500 ps.

The fourth set of parameters in Table I is the Mach numbers. Using the measured plasma flow speed and estimating the electron temperature as $T_e=T_i=180\pm20$ eV enables an estimate of an experimental Mach number. Applying the expansion speed at 500 ps and position 0.5 mm gives an experimental Mach number of 12, approaching the strong shock regime. This experimental result is compared to the simulated Mach number in Fig. 10, which indicates that the Mach number is expected to remain greater than 1 for at least 2 ns. Alfvén Mach number is estimated to be around 20 for the experiment at 500 ps. High Mach numbers and Alfvén Mach numbers are important to ensure that a strong shock is formed.

The two last dimensionless parameters of Table I, the Reynolds and Peclet numbers, are much larger than unity. This is necessary to ensure that dissipative effects are negligible, so that the Euler equations can be applied both to the SNR and to the experiment.

The experimental results of counter-streaming plasmas with magnetic field shown in Figs. 4(b) and 5 are notably different to the field free case, Fig. 4(a). The electron density profiles appear to be altered by the magnetic field. Steepened density gradients separated by an extended, uniform, low-density region are observed in the mid-point of the experiment (indicated as 0 on the horizontal axis in Figs. 4 and 5). This low-density region is also associated with a small, and unusual, increase in density. Given that the plasma $\beta\gg1$ when the image was taken (500 ps), it is difficult to explain the density profile and the small density increases in the central area by a magnetic field retarding the plasma flow, or by magnetic field compression between the leading edges of the two plasmas. The simulated r_{Li}/L with $T_i\sim200$ eV (the thick dashed line in Fig. 9) indicates that the magnetic field inside the plasma due to a 7.5 T external field is sufficient to localize the ions, i.e., $r_{\mathrm{Li}}/L<1$, up to 150 μm from the experimental mid-point. This indicates that counter-streaming experiment, with foil targets separated by 1 mm would have a central area approximately 300 μm wide where $r_{\mathrm{Li}}/L<1$. This width is similar to the measured width of the flat low-density region in Figs. 4(b) and 5. However, we note that simulations indicate that the parameter r_{Li}/L calculated at the position 0.5 mm increases quickly with time and approaches unity at 700 ps for the ions and 900 ps for the electrons.

A magnetic field can indirectly affect the interaction of collision-free counter-streaming flow, for example, through a collisionless coupling. However, we stress such a conclusion requires further study. It appears the magnetic field may penetrate this plasma on a length comparable to the observed central low-density region. As momentum is mainly carried by ions, the most significant collisionless coupling mecha-

nisms would involve the counter-streaming ions. This is a possible explanation for the observed low-density, electron density plateau. The magnetic field has penetrated the plasma and effectively localized the ions, introducing new shorter length scales, namely the ion and electron gyroradius. Experimental ion gyroradius normalized to the system size, is shown in Fig. 9 at 500 ps and at the mid-point between the foil targets. However, we note that many plasma physics processes, operating on different length scales and time scales, are likely to contribute to the observed behavior. For a review of this point in its astrophysical context, we refer to Ref. 19 and references therein. For recent particle-in-cell simulations and analytical discussions of some of the plasma physics processes occurring at SNR shocks, we refer to Refs. 19–22.

These measurements indicate that the necessary requirements for a laboratory study of collisionless physics relevant to a young SNR can be created by a laser plasma experiment. Indeed, the transverse magnetic field is observed to affect the interaction of two counter-streaming plasmas, however no definitive evidence of a shock, collisionless or otherwise has been observed. The most plausible explanation is that the ion localization r_{Li}/L is not sufficient and a value of 10^{-2} is required. This can be investigated in the future with experiments using larger plasmas, this will require working with lower plasma density to ensure the collisionality parameter remains sufficiently high.

VI. CONCLUSION

In this experiment, we have investigated the dynamics of the back surface of an expanding plasma produced from the laser-driven explosion of a thin plastic foil, and in separate experiments the interaction of two counter-propagating plasmas in opposing geometry. This study was carried out without and with a 7.5 T magnetic field orientated transverse to the plasma flow. Experimental and numerical results at 500 ps show that the experimental dimensionless parameters can be matched to those of a reverse shock in a young supernova remnant, and that scaled laser plasma experiments of collisionless astrophysical phenomena is possible. Experimental and numerical results show that the magnetic field is not sufficiently strong to affect the expansion dynamics of a single plasma and that the interaction between the two plasmas is collision free. However, the interaction of two similar counter-streaming plasmas is affected by the presence of the magnetic field transverse in the plasma flow. Compared to the field free case, where the density profile indicates plasma interpenetration, the magnetic field alters the plasma profile in three ways. First, the density profiles are steepened; second an extended low-density region is observed; and third, small density enhancements are observed on either side of the experimental mid-point. Experimental evidence indicates that magnetic compression does not occur. We have suggested that the magnetic field penetrates the plasmas due to ion acoustic turbulence and a resulting anomalous resistivity. Estimates suggest magnetic field penetration of 150 μm. If this occurs, it is possible that the features observed result from a collisionless coupling between the leading edges of the plasmas. Finally, we believe collisionless shock formation can be studied using magnetized counter-streaming laser-produced plasmas. These results indicate that increasing the plasma size and using magnetic fields of the order 10 T are sufficient.

ACKNOWLEDGMENTS

The authors express thanks to Dr. Karl Krushelnick and Imperial College of the loan of the electromagnet, to B. Lings, K. Rosol'anková, University of Oxford, and to Dr. Per Helander for discussions, and to the Central Laser Facility staff.

This work is funded by the UK Engineering and Physical Sciences Research Council.

[1] B. H. Ripin, C. K. Manka, T. A. Peyser, E. A. McLean, J. A. Stamper, A. N. Mostovych, J. Grun, K. Kearney, J. R. Crawford, and J. D. Huba, Laser Part. Beams **8**, 183 (1990).
[2] B. A. Remington, D. Arnett, R. P. Drake, and H. Takabe, Science **248**, 1488 (1999).
[3] H. Takabe, H. Nagatomo, A. Sunahara, N. Ohnishi, A. I. Mahdy, Y. Yoda, S. Naruo, H. Azechi, H. Nishimura, and K. Mima, Plasma Phys. Controlled Fusion **41**, A75 (1999).
[4] S. J. Rose, Phys. World **7**, 56 (1994).
[5] A. Levinson and R. Blandford, Mon. Not. R. Astron. Soc. **274**, 717 (1995).
[6] A. R. Bell, P. Choi, A. E. Dangor, O. Willi, D. A. Bassett, and C. J. Hooker, Phys. Rev. A **38**, 1363 (1988).
[7] D. D. Ryutov, B. A. Remington, and H. F. Robey, Phys. Plasmas **8**, 1804 (2001).
[8] R. Enomoto, T. Tanimori, T. Naito, T. Yoshoda, S. Yanagita, M. Mori, P. G. Edwards, A. Asahara, G. V. Bicknell, S. Gunji, S. Hara, T. Hara, S. Hayashi, C. Itoh, S. Kabuki, F. Kajino, H. Katagiri, J. Kataoka, A. Kawachi, T. Kifune, H. Kubo, J. Kushida, S. Maeda, A. Maeshiro, Y. Matsubara, Y. Mizumoto, M. Moriya, H. Muraishi, Y. Muraki, T. Nakase, K. Nishijima, M. Ohishi, K. Okumura, J. R. Patterson, K. Sakurazawa, R. Suzuki, D. L. Swaby, K. Takano, T. Takano, F. Tokanai, K. Tsuchiya, H. Tsunoo, K. Uruma, A. Watanabe, and T. Yoshikoshi, Nature (London) **416**, 823 (2002).
[9] N. C. Woolsey, Y. Abou Ali, R. G. Evans, R. A. D. Grundy, S. J. Pestehe, P. G. Carolan, N. J. Conway, R. O. Dendy, P. Helander, K. G. McClements, J. G. Kirk, P. A. Norreys, M. M. Notley, and S. J. Rose, Phys. Plasmas **8**, 2439 (2001); R. P. Drake, *ibid.* **9**, 727 (2002); N. C. Woolsey, Y. Abou Ali, R. G. Evans, R. A. D. Grundy, S. J. Pestehe, P. G. Carolan, N. J. Conway, R. O. Dendy, P. Helander, K. G. McClements, J. G. Kirk, P. A. Norreys, M. M. Notley, and S. J. Rose, *ibid.* **9**, 729 (2002).
[10] A. Decourchelle, D. C. Ellison, and J. Ballet, Astrophys. J. Lett. **543**, L57 (2000).
[11] J. W. Connor and J. B. Taylor, Nucl. Fusion **17**, 1047 (1977).
[12] D. Ryutov, R. P. Drake, J. Kane, and B. A. Remington, Astrophys. J. **518**, 821 (1999).
[13] A. Djaoui and S. J. Rose, J. Phys. B **25**, 2745 (1992).
[14] T. E. Stringer, J. Nucl. Energy **6**, 267 (1964).
[15] C. Chenais-Popovics, P. Renaudin, O. Rancu, F. Gilleron, J. C. Gauthier, O. Larroche, O. Peyrusse, M. Dirksmoller, P. Sondhauss, T. Missalla, I. Uschmann, E. Forster, O. Renner, and E. Krousky, Phys. Plasmas **4**, 190 (1997).
[16] J. Aparicio, M. G. Haines, R. J. Hastie, and J. P. Wainwright, Phys. Plasmas **5**, 3180 (1998).
[17] R. M. Kulsrud, Phys. Plasmas **5**, 1599 (1998).
[18] C. E. J. Watt, R. B. Horne, and M. P. Freeman, Geophys. Res. Lett. **29**, L1004 (2002).
[19] R. O. Dendy and J. G. Kirk, Plasma Phys. Controlled Fusion **41**, A427 (1999).
[20] H. Schmitz, S. C. Chapman, and R. O. Dendy, Astrophys. J. **579**, 327 (2002).
[21] M. E. Dieckmann, K. G. McClements, S. C. Chapman *et al.*, Astron. Astrophys. **356**, 377 (2000).
[22] H. Schmitz, S. C. Chapman, and R. O. Dendy, Astrophys. J. **570**, 637 (2002).